Materials Advances

ROYAL SOCIETY OF CHEMISTRY

PAPER

View Article Online
View Journal | View Issue



Cite this: *Mater. Adv.*, 2026, 7, 2426

# Application of carboxylated carbon nanotubes as artificial channels to facilitate *n*-decane transport through bacterial cell membranes

Sara Yazdani, *[a] Davoud Biria*[a] and Gholamreza Pazuki [b]

Received 21st September 2025,
Accepted 8th January 2026

DOI: 10.1039/d5ma01079a

rsc.li/materials-advances

Facilitating the transport of hydrocarbons across bacterial cell membranes can improve the efficiency and rate of bioremediation processes. In this study, we evaluated the potential of carbon nanotubes (CNTs), particularly functionalized CNTs (CNT–COOH), as artificial membrane channels to enhance the uptake of hydrophobic compounds into bacterial cells. The toxicity of CNTs was firstly assayed using *Bacillus subtilis* and *Pseudomonas aeruginosa* strains, and the obtained results revealed that the toxicity of carboxylated CNTs was reduced significantly. Molecular dynamics simulations further confirmed a stable CNT integration into the bilayer membrane model in terms of interaction energies. Our results suggested that a short (around 10 nm), carboxylated CNT system would adopt a perpendicular alignment to the membrane, thus forming an artificial channel. Hydrocarbon uptake experiments using *n*-decane demonstrated enhanced internalization in the presence of CNT–COOH, with intracellular *n*-decane levels increasing by 32% and 41% for *B. subtilis* and *P. aeruginosa*, respectively, in comparison with the blank tests. It was disclosed that the CNT–COOH can be used as an effective tool for constructing nanoscale membrane channels to increase hydrocarbon transport into bacterial cells for bioremediation applications.



## 1. Introduction

The plasma membrane is the outermost layer of the cell structure that separates the internal medium of the cell from the external environment. It mainly consists of a phospholipid bilayer with embedded proteins that have specific functions.[1] This membrane plays several crucial roles, including protecting the cell, maintaining a stable internal environment, and regulating the transport of nutrients and waste products into and out of the cell. Membrane proteins enable the transport of materials through the cell membrane and facilitate interactions with other cells. Effective monitoring and control of materials movement into cells is a key aspect of bioengineering. Specifically, the efficient transport of hydrophobic substances, such as certain anticancer drugs (doxorubicin, paclitaxel, and docetaxel), through the cell membrane—acting as the first barrier—is a major concern in biomedicine and drug delivery.[2] In fact, delivery of hydrophobic drugs into the targeted cells in significant quantities and within a short time is important to achieve an effective response. However, the poor permeability of these materials through the targeted cell wall impedes this process, making hydrophobicity a critical factor in membrane permeability.[3] Similarly, for the successful degradation of hydrophobic pollutants (*e.g.*, petroleum hydrocarbons) by microorganisms, it is essential to intensify the cellular uptake of these compounds to improve the kinetics of the biodegradation process. Numerous microorganisms such as the hydrocarbon assimilating bacteria, with their diverse metabolic capabilities, participate in their degradation and considered as the basis of several effective biological processes for mitigating environmental pollutions caused by oil spills and industrial activities.[4,5] However, the slow rate of uptake and degradation of these materials by the bacteria and their low solubility in the aqueous phase are among the important factors that adversely affect the efficiency of bio-based processes. While the application of surfactants and increasing the two-phase interface area can enhance the mass transfer of hydrophobic materials to the cells, the challenge of transferring these substances through the cell membrane remains a significant obstacle.

Nanotechnology presents promising methods for overcoming the challenges associated with delivering hydrophobic substances into cells. For instance, CNTs with their distinctive cylindrical shape and advantageous physicochemical traits[6,7] have emerged as effective tools for this purpose. Nanotubes can either directly pass through cell membranes or enter cells *via* endocytosis and phagocytosis when modified with

[a] *Department of Chemical Engineering, University of Isfahan, Isfahan 8174673441, Iran. E-mail: s.yazdani@eng.ui.ac.ir, d.biria@ast.ui.ac.ir*
[b] *Department of Chemical Engineering, Amirkabir University of Technology, Tehran, Iran*

biocompatible substances. On the other hand, they can be used to form artificial porin like channels in the cell membrane.[8,9] These channels can be specifically tailored to facilitate the uptake of hydrophobic materials such as petroleum hydrocarbons into cells.[10] In fact, a system that consists of a bacterial membrane and hydrocarbons can be considered as a simple and cost-effective arrangement to evaluate the application of CNTs as artificial membrane channels.[10–12]

Despite their great potential, there are unresolved issues regarding how CNTs interact with cells, highlighting the urgent need for in-depth and precise studies on the physical and chemical interactions that trigger a biological response. It has been frequently reported that CNTs have cytotoxic effects, which is a great drawback for their application in living systems. Moreover, the orientation of CNTs and their stability within the cell membrane are important prerequisites to form artificial membrane channels. Currently, a significant amount of experimental data related to the biomedical applications of CNTs is available. However, the discrepancies in experimental results suggest that this information is incomplete. In some instances, CNTs have been reported as excellent intracellular delivery carriers for certain drugs,[13,14] while in other scenarios, they exhibit high toxicity.[15,16] Modification of CNTs by the addition of appropriate functional groups to their surface has been suggested as the most practical solution to the mentioned problems.[17–19]

A lipid bilayer, in addition to its self-assembling properties,[20] possesses other characteristics such as fluidity and deformability,[21] which are essential for many membrane functions. Therefore, evaluating the hydrophobic/hydrophilic interactions between CNTs and bacterial cell membranes and studying changes in the mechanical properties of CNT complexes with bacterial cell membranes are crucial for enhancing the permeability of hydrocarbons into cells.

In light of the above, the present article aims at investigating the effectiveness of CNTs as artificial membrane channels to improve the uptake and biodegradation of hydrocarbons by the bacterial species. The cytotoxicity of the pristine and carboxylated single-walled CNTs on the bacterial cells was examined. The dynamic interactions of CNTs with a lipid bilayer as a model of the cell membrane was studied to ensure the proper orientation of the functionalized CNTs within the cell membrane. These interactions were analyzed experimentally to approve the results of the molecular dynamics simulations. Finally, the changes in the uptake and degradation of a hydrocarbon material (*n*-decane) into the bacterial cells as a result of treatment with CNTs were assayed.

## 2. Materials and methods

Pristine CNTs and CNT–COOH were purchased from NanoCs (USA). Commercial single-walled carbon nanotubes from NanoCs typically possess diameters of 2–10 nm, lengths of 50 $nm^{-1}$ μm, and >95% carbon purity, which are consistent with the common physicochemical features reported for high-purity SWCNTs synthesized by CVD methods.[22–25] 1,2-Distearoyl-*sn-glycero*-3-phosphoethanolamine-N [carboxy(polyethylene glycol)-2000] (DSPE-PEG (2000)-COOH) was purchased from NOF Sunbright (USA). Nutrient broth, nutrient agar, and Bushnell Haas (BH) broth powder culturing media were purchased from Ibresco (Iran). Tween 80, phosphate-buffered saline (PBS), and Triton X-100 were sourced from Merck, Germany. Normal decane and chloroform used in this study were purchased from Sigma-Aldrich (USA). The employed bacteria (*Bacillus subtilis* and *Pseudomonas aeruginosa)* were isolated from an oil-contaminated soil sample and deposited with accession numbers KC309409 and JX163115 in the GenBank database, respectively.[26] Distilled water was used in all experiments.

### 2.1. Preparation of suspensions with different types of CNTs

Polyethylene glycol-functionalized CNTs (FCNTs) were synthesized according to the method described by Yazdani *et al.*[27,28] To investigate the influence of various types of CNTs (*i.e.*, pristine and functionalized) on the bacterial growth and the membrane permeability, the CNT powder was suspended in the aqueous phase. 10 mg of each type of CNTs were dispersed in 10 mL of Tween 80 in separate vials using an ultrasonic bath for 1 hour. In the next step, 6 mL of the pristine CNT, CNT–COOH, and FCNT solutions were added to 100 mL of nutrient broth medium in three Erlenmeyer flasks and incubated at 37 °C and 120 rpm for 3 hours. This incubation step was performed to allow the initial interaction between the CNTs and the culture medium.[22,23] Dispersion of CNTs in Tween-80 is well established to generate stable individualized nanotube suspensions and prevent aggregation.[29,30] These reported parameters align with CNTs used in prior biological and membrane interaction studies.

### 2.2. Bacterial culturing media and growth conditions

The nutrient broth medium was prepared by dissolving its powder in distilled water at a concentration of 13 g $L^{-1}$. The BH medium was prepared by adding 3.27 grams of BH powder into 1 L of distilled water. All culturing media were sterilized (121 °C, 20 min) before use in the experiments. Each of the bacterial strains *(Bacillus subtilis* and *Pseudomonas aeruginosa)* was inoculated into 250 mL Erlenmeyer flasks containing 100 mL of the nutrient broth medium to prepare a pre-culturing broth. The flasks were incubated at 37 °C and 160 rpm for 24 hours in a rotary shaker. Then the bacterial cell density was assayed through the enumeration of colony forming units (CFU) on the nutrient agar Petri dishes. The obtained bacterial broth was used for inoculating the culturing media in the following experiments (*i.e.*, toxicological studies, orientation of CNTs in bacterial membranes, and examination of the effect of CNTs on the hydrocarbon uptake by the bacteria). The inoculum volume was adjusted to achieve the desired cell density in each experimental setup.[27,31]

### 2.3. Effect of CNTs on the bacterial growth and viability

The effect of pristine and functionalized CNTs on the growth rate of the bacterial strains *Bacillus subtilis* and *Pseudomonas aeruginosa* was investigated. The bacteria were cultured in 7 mL

of the nutrient broth medium at 37 °C for 24 hours, as described by Chen *et al.*,[32] to achieve a population density of $1.2 \times 10^8$ and $2.0 \times 10^9$ cells per mL for each bacterial species, respectively. The obtained cultures were then diluted by the addition of certain volumes of three types of CNT solutions: FCNT, commercial CNT–COOH, and pristine CNT. These mixtures were incubated at 37 °C in a shaker incubator at 160 rpm for 3 h. For each type of CNT (pristine, CNT–COOH, and FCNT), the final concentrations in the culture medium were set at 7.5, 15, 30, 60, and 120 μg $mL^{-1}$. A flask without CNTs served as the control to observe the normal growth of the bacterial cells. The samples were arranged in 96-well plates. Prior to use, the plates were sterilized using the procedure described by Rogers *et al.*[33] To monitor bacterial growth, the 96-well plates were placed in a microplate reader (ELISA reader model 800TS, Arena Gen Tehiz, Iran), and the optical density (OD) of each well was measured at 600 nm every 30 minutes for 48 hours.[34]

To examine the influence of CNTs on the bacterial population, following the methodology reported by Chatterjee *et al.*,[35] the population density obtained from the pre-cultures of *Bacillus subtilis* and *Pseudomonas aeruginosa* were inoculated into the nutrient broth medium containing various amounts of pristine CNTs, CNT–COOH, and FCNTs. A control sample, cultured under identical conditions but without CNTs, was also prepared. At specific time intervals, aliquots of the cultures were taken and sequentially diluted with PBS. These diluted suspensions were then spread on nutrient agar plates and incubated at 37 °C for 24 hours, after which the colonies were counted. Experiments were performed in triplicate, and the colony counts for each set were averaged.[35,36] The bacterial population was calculated using the number of colonies and the dilution factor according to eqn (1):

$$\text{CFU per mL of a sample} = \text{the number of colonies} \times \text{the dilution factor of the plate counted} \quad (1)$$

### 2.4. Interactions between the bacterial cell membrane and CNTs

Transmission electron microscopy (TEM) is a powerful and widely used technique for the structural and morphological characterization of nanoscale materials. In this study, TEM was employed to visualize and analyze the interactions between carboxyl-functionalized carbon nanotubes (CNT–COOH) and bacterial cells. High-resolution TEM was used to examine the orientation and localization of CNTs relative to the bacterial cell envelope, providing insights into their potential insertion into or association with the cell. For sample preparation, a portion of the culture medium containing either *Bacillus subtilis* or *Pseudomonas aeruginosa* was transferred into 15 mL vials. Subsequently, CNT–COOH were added into individual vials to achieve a final CNT concentration of 60 μg $mL^{-1}$. According to our preliminary findings, a concentration of 60 μg $mL^{-1}$ was identified as the optimal condition for subsequent experiments, balancing the incorporation of CNTs into the bacterial culture with the preservation of cell viability. In fact, cells exposed to this concentration maintained an acceptable viability level compared to other tested concentrations, justifying the selection of this dose for further analyses. Each vial contained either *Bacillus subtilis* or *Pseudomonas aeruginosa* along with the carboxylated CNTs. The vials were then incubated at 37 °C for 2 hours at 160 rpm. After that, the samples were subjected to freeze-drying (lyophilization) for 24 hours at low temperature to fix the interactions of CNTs with the bacterial cell membranes. A drop of each sample was placed onto a copper TEM grid coated with a Holley carbon film. Bright-field TEM images were obtained using a Philips CM120 transmission electron microscope (Philips, The Netherlands) operated at an accelerating voltage of 200 kV.

### 2.5. Modelling the membrane cell interactions with CNTs by molecular dynamics simulations (MDS)

The simulation system included a fully hydrated lipid bilayer, containing either pristine CNTs or CNT–COOH, along with 3 mol% of carbon dioxide ($CO_2$) and urea molecules. $CO_2$ and urea served as representatives of small hydrophobic and hydrophilic molecules, respectively, suitable for transport through CNT channels. The fraction of these molecules was calculated as the ratio of $CO_2$ or urea molecules to the sum of the $CO_2$ or urea and water molecules and reported as mole percent. The hydrated bilayer was composed of 118 dipalmitoylphosphatidylcholine (DPPC) lipids and roughly 4500 water molecules. Armchair-type CNTs (6,6) and (7,7), each approximately 3.9 nm in length, corresponding to the membrane thickness, were used for both pristine and functionalized nanotubes. CNT–COOH were prepared by attaching 12 carboxylic acid groups to the terminal carbon atoms at both ends of CNTs. The force field parameters for DPPC lipids were taken from Berger *et al.*,[37] while those for CNTs were taken from Hammer *et al.*[38] $CO_2$ and urea topologies were created using the PRODRG server based on the GROMOS53a6 force field.[39] The van der Waals (vdW) parameters for $CO_2$ and urea were incorporated from GROMACS, and water molecules were represented by the SPC model.[40] Carbon atoms in the pristine CNTs were modeled as uncharged Lennard-Jones (LJ) spheres, with a cross-sectional diameter ($\sigma_{cc}$) of 0.38 nm and a potential well depth ($\varepsilon_{cc}$) of 0.40 kJ $mol^{-1}$. Simulations were performed under the isobaric–isothermal (NPT) ensemble using the GROMACS 4.5.6 software package.[41,42] Periodic boundary conditions were applied in all directions. The vdW interactions were treated with a smooth cut-off at 1 nm, and the Ewald particle mesh method was used for calculating long-range electrostatic interactions.[43,44] Bond lengths within CNTs, DPPC, and water molecules were constrained using the LINCS and SETTLE algorithms, allowing for a 3 fs time step.[45,46] Initial steered MDS were conducted to move the molecules from the aqueous phase to the center of mass of the membrane or CNTs.[47] Following this, 35 windows were created along the reaction coordinate (*z*-direction), with the *z*-coordinate of the center-of-mass (COM) distance between the molecule and the membrane or CNT varying by approximately 0.1 nm in each window to ensure adequate sampling.

Each window was simulated for 10 ns, with the final 5 ns used for data collection.[48] All simulations were run on an Ubuntu operating system with GPU acceleration (90 30 GPU). The MDS were conducted to investigate how surface functionalization of carbon nanotubes with carboxylic acid groups (CNT–COOH) affects their interaction with lipid bilayers and their potential to mediate the transport of small molecules. It was anticipated that CNT–COOH, due to their polar functional groups, would exhibit stronger interactions with the hydrophilic head groups of membrane lipids compared to pristine CNTs, possibly altering their orientation and insertion depth within the bilayer. These simulations were intended to provide mechanistic insight into how functionalization modulates CNT behavior in a biological membrane environment and impacts their potential use as nanocarriers or membrane-penetrating agents.

### 2.6. Measurement of hydrocarbon infiltration into cells

After preparing the nutrient broth medium and reaching a cell population of approximately $10^8$ cells per mL for each of the bacterial strains (*i.e.*, *Bacillus subtilis* and *Pseudomonas aeruginosa*), the microbial cells were separately harvested from the media using centrifugation (10 000 rpm) at 4 °C and added to 100 mL of sterilized Bushnell–Haas mineral medium. Then, each flask was supplemented with approximately 2% (v/v) *n*-decane and incubated at 37 °C and 160 rpm for 12 hours. Next, the CNT samples (pristine CNTs or CNT–COOH) at a concentration of 60 μg $mL^{-1}$ were separately added to the microbial broth and incubated for 12 hours at 37 °C and 160 rpm. After that, the resultant broth was centrifuged at 4 °C for 20 minutes at 9000 rpm. At this stage, the bacterial cells mostly settled at the bottom of the Falcon tubes, while the remaining hydrocarbons were present in the supernatant. The hydrocarbons were separated from this supernatant through mixing with 5 mL of chloroform. The mixture was then vigorously shaken to ensure the proper extraction of hydrocarbons into the chloroform phase. Meanwhile, 5 mL of sterile distilled water was added to the cells adhered to the bottom of the Falcon tube, and the mixture was placed in an ultrasonic bath for 90 minutes to break the cell walls and release the internalized hydrocarbons within the bacterial cells. The hydrocarbons in this mixture were then extracted with 1 mL of chloroform, and after phase separation, the amounts of hydrocarbons in the lower phase were determined using a gas chromatography (GC) apparatus (Agilent, USA) equipped with an HP-5 column and a flame ionization detector (FID). The column had a length of 30 meters and an internal diameter of 0.32 mm. Nitrogen was employed as the carrier gas at a flow rate of 0.6 mL $min^{-1}$, and the inlet pressure of the column was set to 5.77 psi. The column temperature was maintained at 85 °C for 10 minutes. This process was performed for both bacterial strains using two different types of carbon nanotubes (pristine and CNT–COOH). Four control experiments including two non-microbial controls (free of bacterial strains, with CNTs) and two microbial controls free of carbon nanotubes were conducted as well. Non-microbial control systems were used to observe the effect of carbon nanotubes on hydrocarbons in the absence of bacteria, while microbial control systems were employed to examine the direct interaction of bacteria and hydrocarbons in the absence of carbon nanotubes. Another control without any bacteria or CNTs was considered to ensure the influence of the studied factors on hydrocarbon uptake and degradation. These controls enabled us to accurately evaluate the unique effects of the studied factor.

### 2.7. Statistical analysis

All experimental data were obtained from at least three independent replicates and are expressed as mean ± standard deviation (SD). Statistical differences between groups (*e.g.*, control, pristine CNTs, CNT–COOH, and FCNTs) were analyzed using one-way analysis of variance (ANOVA). A *p*-value of less than 0.05 was considered statistically significant. All statistical analyses and graphical representations were performed using OriginPro software.

## 3. Results and discussion

### 3.1. Investigation of the structure of functionalized CNTs

Raman spectroscopy is used in this study for the quantitative investigation of the structural variations and properties of CNTs in three different states – pristine CNTs, CNT–COOH, and FCNTs[49] – based on the Raman shift of D- or G-bands and the G-band to D-band intensity ratio ($I_G/I_D$). The D-band indicates the presence of structural defects and disordered sites on the surface of CNTs and is commonly associated with impurities. It typically appears at around 1331 ± 25 $cm^{-1}$.[50,51] The G-band is associated with the tangential vibration mode of carbon atoms and it usually appears at 1550–1600 $cm^{-1}$.[51,52] The Raman spectra of CNTs, CNT–COOH and FCNTs are shown in Fig. 1. In the Raman spectrum, the pristine CNTs' specified D-band and G-band peaks were observed at 1345 $cm^{-1}$ and 1583 $cm^{-1}$, respectively. Also, a clear peak at 2671 $cm^{-1}$ related to the G'-band was observed, which is related to the second ordered process or radial movement of carbon atoms, and appeared to be close to twice the size of the D band. In FCNTs, the peaks of the D-band, G-band and G′-band shifted to 1345 $cm^{-1}$, 1585 $cm^{-1}$ and 2680 $cm^{-1}$, respectively. The $I_G/I_D$ ratio decreased from 9.16 (pristine CNTs) to 3.04 (FCNTs). If the $I_G/I_D$ ratio was low, more defects would exist on its surface, which is an indication that there are several functional groups added onto the surface of CNTs. The obtained results are consistent with previous studies.[53,54] Thakur *et al.*[55] functionalized MWCNTs with carbohydrate ligands, such as galactose, mannose, and lactose, using lysine as a linker. Raman analysis of various functionalized CNTs showed that the $I_D/I_G$ ratio varied between 0.75 and 0.94, indicating the presence of different functional groups, such as chlorine and lysine, on the surface of the carbon nanotubes. Peon-Diaz *et al.*[56] synthesized CNTs *via* chemical vapor deposition and oxidized them in a mixture of sulfuric acid and nitric acid to create nitrogen and oxygen functional groups. Raman analysis of the carbon nanotube samples showed that the $I_D/I_G$ ratio increased from

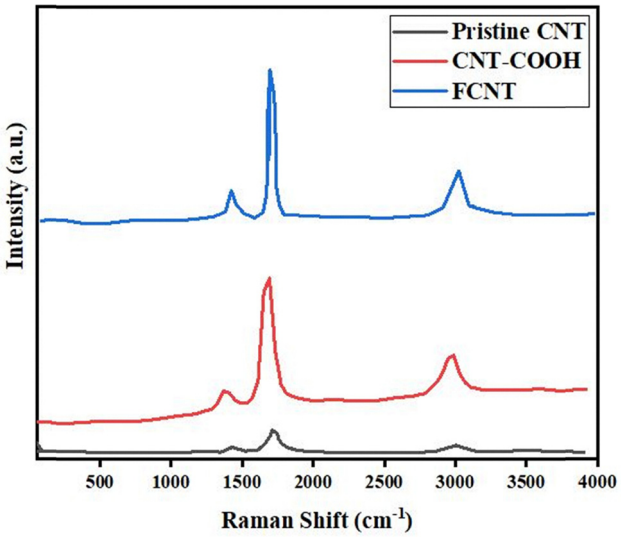


Fig. 1 Raman analysis diagram for pristine CNTs, CNT–COOH, and FCNTs.

1.14 for pristine CNTs to 1.19, 1.20, and 1.24 after surface modification, confirming the presence of functional groups on the surface of the CNTs.

### 3.2. Effects of CNTs on the bacterial density

The bacterial growth in the presence of CNTs was assayed to study the toxic effects of CNTs on the bacteria and the obtained results are shown in Fig. 2 and 3 for *Bacillus subtilis* and *Pseudomonas aeruginosa*, respectively. As can be seen, the growth of bacteria exhibited a typical sigmoidal pattern in all experiments characterized by an exponential increase that peaked after approximately 10–12 hours, followed by a stationary phase or decline over time. Addition of CNTs to the culturing medium decreased the maximum cell density and the concentration of CNTs had an inverse effect on this term for all types of the employed CNTs. The suppressive effect of pristine CNTs was superior to those of CNT–COOH and FCNTs as it significantly reduced the maximum cell population for both bacteria even at the lowest applied concentration (7.5 μg $mL^{-1}$). This suggests that the modification of CNTs with appropriate functional groups could reduce their toxicity to the bacterial cells significantly. The growth of bacterial cells in the medium containing FCNTs was slightly greater than in the CNT–COOH system, which can be explained by the biocompatibility of the PEG moiety in the FCNTs. The large PEG on the surface of CNTs can inhibit their penetration into the cell membrane, thus reducing their toxic effect. However, for employing CNTs as artificial membrane channels, this should not be considered as an advantage. Moreover, the results demonstrated that *Pseudomonas aeruginosa* exhibited a higher resistance to CNTs than *Bacillus subtilis*. For instance, after about 12 hours, at a concentration of 60 μg $mL^{-1}$, the cell density of *Pseudomonas aeruginosa* reached approximately $1.5 \times 10^9$ cells per mL for the CNT–COOH system and $1.3 \times 10^9$ cells per mL for pristine CNTs, whereas that of *Bacillus subtilis* was around $6.7 \times 10^7$ cells per mL in CNT–COOH and $3.8 \times 10^7$ in the presence of CNTs. This means that the viability of *Pseudomonas aeruginosa* and *Bacillus subtilis* cells treated with CNT–COOH was around 13% and 40% higher than those of cells exposed to pristine CNTs, respectively.

This disparity may be attributed to the Gram-negative nature of the *Pseudomonas aeruginosa* membrane, whereas *Bacillus subtilis* is a Gram-positive strain. The obtained results align well with those of previous research.[57–59] Chen *et al.*[32] investigated the antibacterial activity of CNTs with different diameters, lengths, and chemical surface modifications against common intestinal bacteria. They found that the integrity of the bacterial cell membrane decreases due to direct contact between CNTs and the bacterial cell wall, leading to fatal damage to the bacteria. This mechanism is influenced by both the physicochemical and structural properties of the CNTs (*e.g.*, their diameter, surface functional groups, length, and catalytic residues) and the morphology of the bacteria. Their study indicated that thin, rigid SWCNTs were more effective at perforating the cell walls of spherical bacteria. Saleemi *et al.*[60,68] studied the antimicrobial activity of CNTs, particularly double-walled nanotubes and MWCNTs, against pathogenic strains such as Gram-positive *Staphylococcus aureus*, Gram-negative *Pseudomonas aeruginosa*, *Klebsiella pneumoniae*, and various fungal strains. They also investigated the dispersion ability of different CNTs functionalized with the surfactant sodium dodecylbenzene sulfonate (SDBS) and its effect on microbial growth inhibition. They reported that CNTs in bundle form were generally ineffective against pathogens and that the antimicrobial activity of CNTs was influenced by their larger diameter and poor solubility in suspension compared to the functionalized CNTs. Proper dispersion of CNTs was crucial for effective interaction with pathogens. Abo-neima *et al.*[61] explored the antimicrobial activity of MWCNTs as alternative antimicrobial agents compared to commercial antibiotics. They evaluated the antibacterial activity of functionalized CNTs against *Escherichia coli* and *Staphylococcus aureus*, concluding that the optimal concentrations for maximum inhibition were 80 μg $mL^{-1}$ for *E. coli* and 60 μg $mL^{-1}$ for *S. aureus*. To employ CNTs as effective artificial membrane channels, effective interactions between the CNTs and the bacterial cell membrane are important, and at the same time, these interactions should not lead to extensive cell death and loss of the bacterial population. Properly adjusting the concentration of CNTs will supply the system with sufficient effective interactions between the cells and CNTs to facilitate the formation of membrane channels, while avoiding disintegration of the bacterial cell wall due to excessive interactions. Based on the obtained results, a 60 μg $mL^{-1}$ concentration of CNT–COOH was selected for the rest of the experiments in this work. At this concentration, the maximum cell density was around half that of the blank samples, which was still high enough to maintain sufficient viable cells and effective interactions with the CNTs.

Antibacterial assays were carried out on nutrient agar plates containing 7.5–120 μg $mL^{-1}$ of the three types of CNTs (pristine CNTs, CNT–COOH, and FCNTs) for *Bacillus subtilis* and *Pseudomonas aeruginosa*. Approximately $10^7$ colony forming

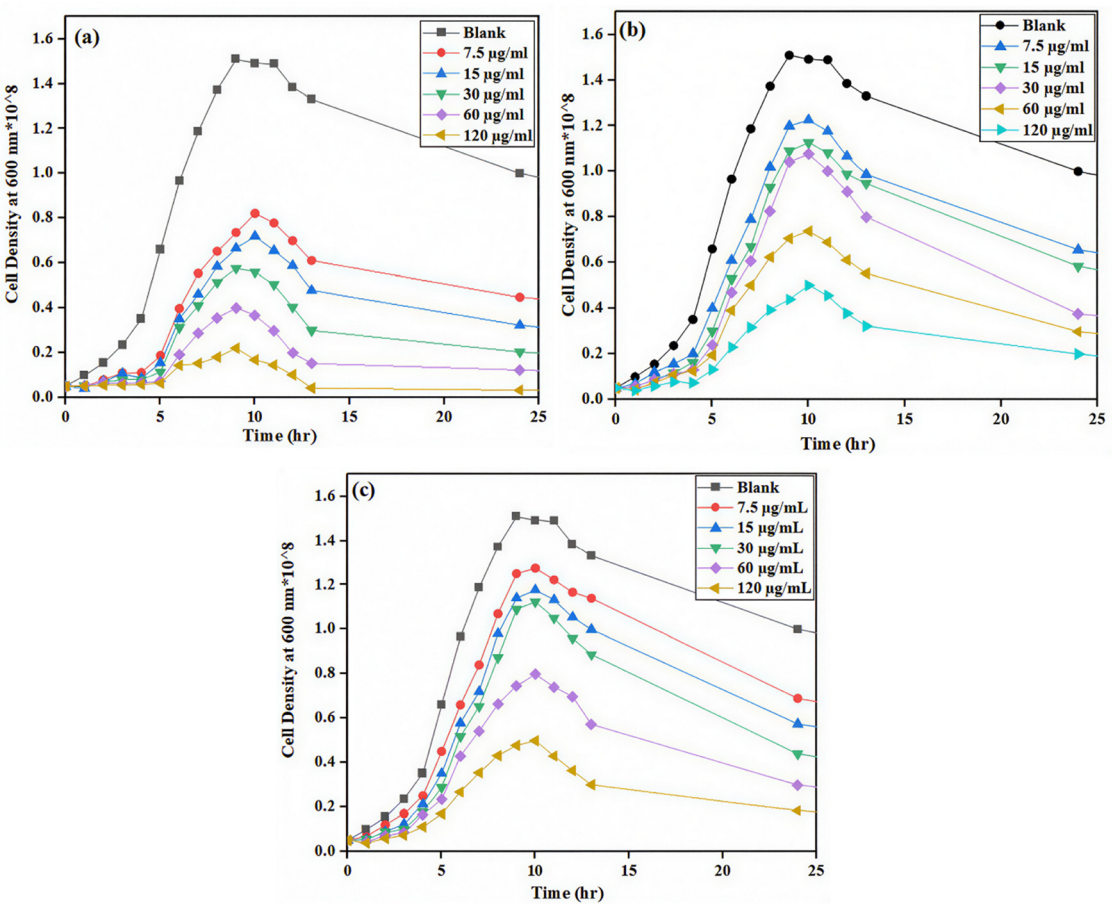


Fig. 2 Growth curves of the *Bacillus subtilis* strain over 24 h with the three types of CNTs: (a) pristine CNTs, (b) CNT–COOH, and (c) FCNTs.

units (CFU) per mL of cells were applied to both control (without CNTs) and the three CNT treated plates. The number of bacterial colonies decreased considerably in the presence of pristine CNTs. Tables S1 and S2 in the SI present the relationship between CFU $mL^{-1}$ and cell density at 600 nm for the control system (without CNTs) and the three systems including pristine CNTs, CNT–COOH and FCNTs with different concentrations ranging from 7.5 μg $mL^{-1}$ to 120 μg $mL^{-1}$. These results highlight that although pristine CNTs exhibit stronger antibacterial activity, surface-functionalized CNTs such as CNT–COOH and FCNTs show reduced cytotoxicity, making them more suitable for applications involving interactions with viable bacterial cells, such as artificial membrane channels.

### 3.3. Visualization of the interactions between CNTs and cell membranes by TEM

Fig. 4 and 5 present the results of TEM analysis of the samples containing CNT–COOH at a concentration of 60 μg $mL^{-1}$ for *Pseudomonas aeruginosa* and *Bacillus subtilis*, respectively. Significant morphological changes were observed on the surface of *Pseudomonas aeruginosa* (Fig. 4) and *Bacillus subtilis* (Fig. 5) bacteria after interaction with CNT–COOH. The CNT structures appeared directly on the cell membrane surface at the center of the small grey granules (indicated by arrows in figures).[62,63] These morphological changes can be attributed to secretion of anti-inflammatory agents by the cells (*e.g.*, exopolysaccharides) to counteract the negative effects of CNTs,[64] particularly in the case of *Pseudomonas aeruginosa*, where signs of membrane irregularity and surface roughness were more pronounced compared to the smoother and more intact membrane of *Bacillus subtilis*. This observation indicates a differential interaction pattern likely rooted in differences between Gram-negative and Gram-positive bacterial membrane architecture. Abunima *et al.*[61] reported morphological changes in *Escherichia coli* and *Staphylococcus aureus* following exposure to CNTs. In *E. coli*, a Gram-negative bacterium, interaction with CNTs led to alterations such as roughened cell walls, disrupted membrane integrity, and cytoplasmic leakage, with CNTs visible as black granules within the membrane. Similarly, CNT-treated *S. aureus* cells (Gram-positive) showed disrupted cytoplasmic structure and membrane damage compared to the smooth and intact morphology of control cells. These observations confirm that both Gram-positive and Gram-negative bacteria can be affected by CNTs, although the extent and nature of the damage may vary depending on the structural properties of their cell walls. TEM images indicate close association between CNTs and membrane surfaces but cannot resolve a full membrane-spanning structure due to inherent limitations of ultrathin sectioning.

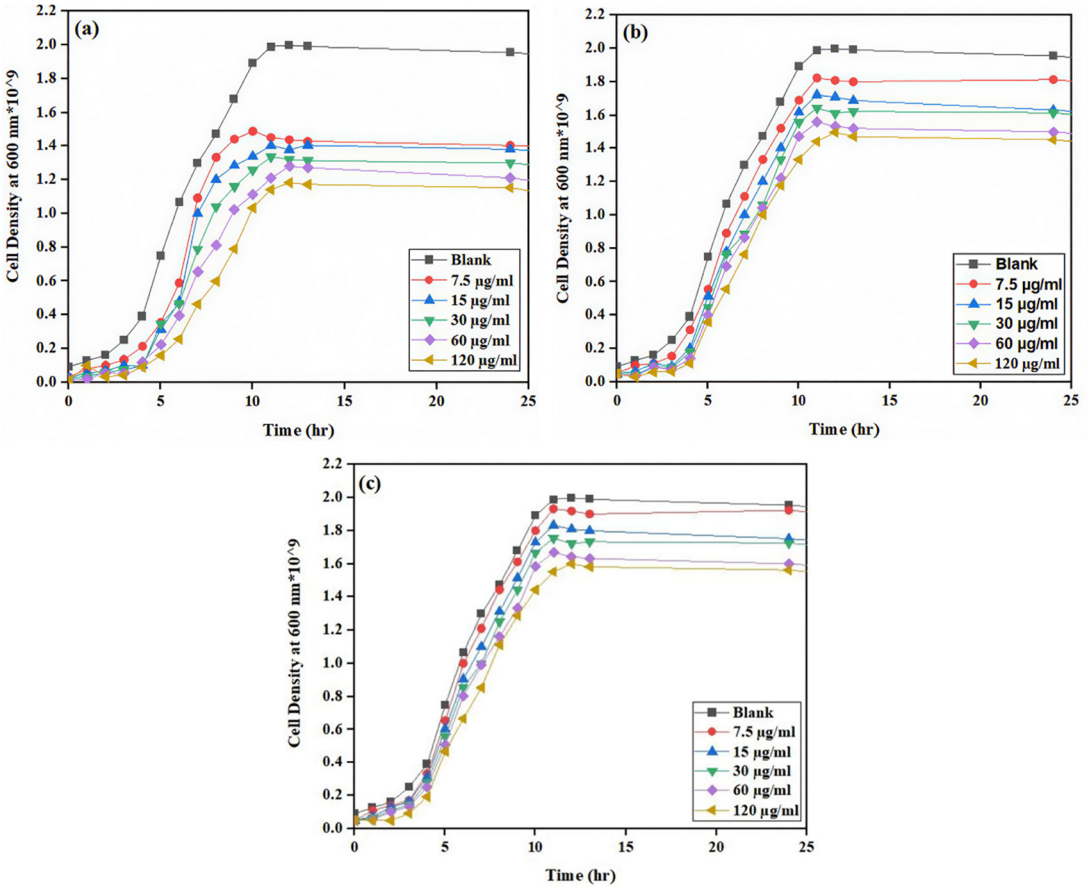


Fig. 3 Growth curves of the *Pseudomonas aeruginosa* strain over 24 h with the three types of CNTs: (a) pristine CNTs, (b) CNT–COOH, and (c) FCNTs.

### 3.4. Modelling of the membrane interactions with CNTs

Fig. 6(a) depicts the visual simulation results illustrating the penetration of CNT–COOH from the aqueous phase into the lipid bilayer in a 120 ns time span. The process begins with the rapid adsorption of CNT–COOH at the lipid bilayer–water interface in a direction parallel to the membrane plane, followed by their spontaneous inclination to embed within the membrane. As illustrated in Fig. 6(a), CNT–COOH are initially drawn swiftly towards the bilayer. At critical times ($t$ = 30 ns and $t$ = 31 ns), they are pulled diagonally into the membrane. Once inside, CNT–COOH remain in an inclined position within the membrane ($t$ = 120 ns), maintaining membrane integrity without causing any tearing, which shows that the modified CNTs can function as artificial channels. CNT–COOH exhibit a different behavior when interacting with the lipid bilayer. We embedded CNT–COOH both vertically and horizontally at the lipid bilayer center and then the simulation started. As depicted in Fig. 6(b), CNT–COOH maintain an almost vertical orientation throughout the simulation (both vertical and horizontal at the membrane center). Specifically, the CNT–COOH in Fig. (6b, right) rotated from a horizontal to a vertical state, with the tilt angle increasing due to electrostatic interactions. Functionalizing CNTs with hydrophilic groups such as carboxyl (−COOH) and hydroxyl (−OH) groups enhances their interaction with the polar head groups of the lipid bilayer. This functionalization facilitates their stable incorporation into the membrane and prevents aggregation, a common issue with pristine CNTs.[17,29] The presence of these functional groups increases the hydrophilicity of the CNTs, allowing for better dispersion in aqueous environments and improved compatibility with biological membranes.[29,65,66] Additionally, the electrostatic interactions between the functional groups on the CNTs and the lipid head groups stabilize the vertical orientation of the functionalized CNTs, enhancing their potential as conduits for molecular transport across the membrane. These characteristics make functionalized CNTs more effective and reliable as nanoscale channels for various applications, including drug delivery and biosensing.

To investigate the effects of CNT length on the lipid membrane insertion process, three additional independent simulations were performed using pristine CNTs of varying lengths: 2.6 nm, 3.8 nm, and 5 nm, which are shorter than, comparable to, and longer than the thickness of the lipid bilayer, respectively. As shown in Fig. 7, CNTs that were shorter or approximately equal to the thickness of the lipid bilayer underwent significant rotation and tended to position themselves vertically within the center of the bilayer. It is important to note that the final orientation of pristine CNTs is influenced by their initial structure. As the length of the CNTs

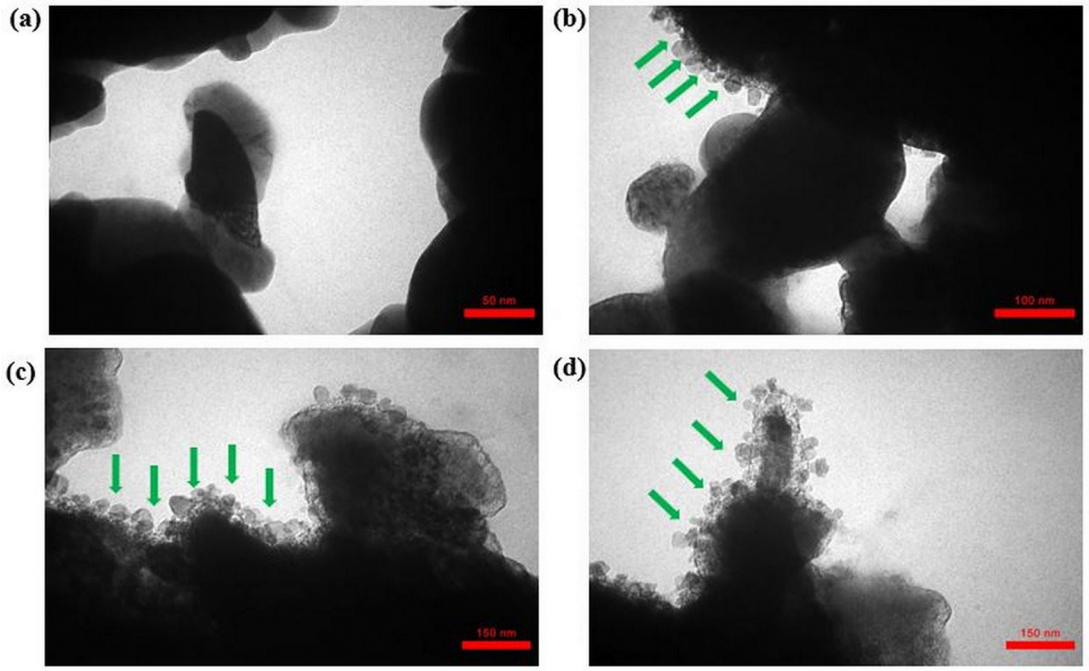


Fig. 4 TEM images of (a) *Pseudomonas aeruginosa* samples without CNTs (blank) at 50 nm magnification and (b)–(d) *Pseudomonas aeruginosa* samples with CNT–COOH at 60 μg $mL^{-1}$ after 24 hours of incubation, shown at 100 nm and 150 nm magnifications.

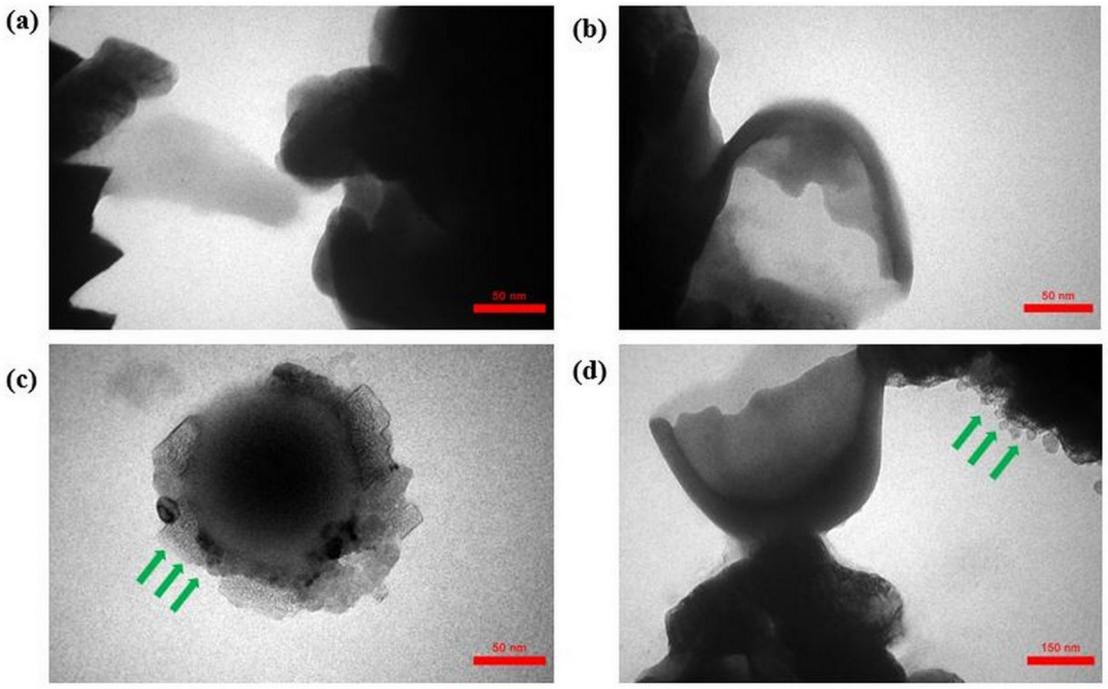


Fig. 5 TEM images of (a) and (b) *Bacillus subtilis* samples without CNTs shown at 50 nm magnification and (c) and (d) *Bacillus subtilis* samples with CNT–COOH at 60 μg $mL^{-1}$ after 24 hours of incubation, shown at 50 nm and 150 nm magnifications.

increased, their ability to rotate diminished, as longer CNTs were more prone to confinement within the membrane. The orientation of CNTs in the cell membrane is crucial for their function as potential channels for molecular transport. Shorter CNTs, due to their smaller size, can easily rotate and align themselves perpendicularly to the membrane, facilitating the formation of stable, vertical channels. These channels can effectively span the entire thickness of the bilayer, providing a continuous pathway for

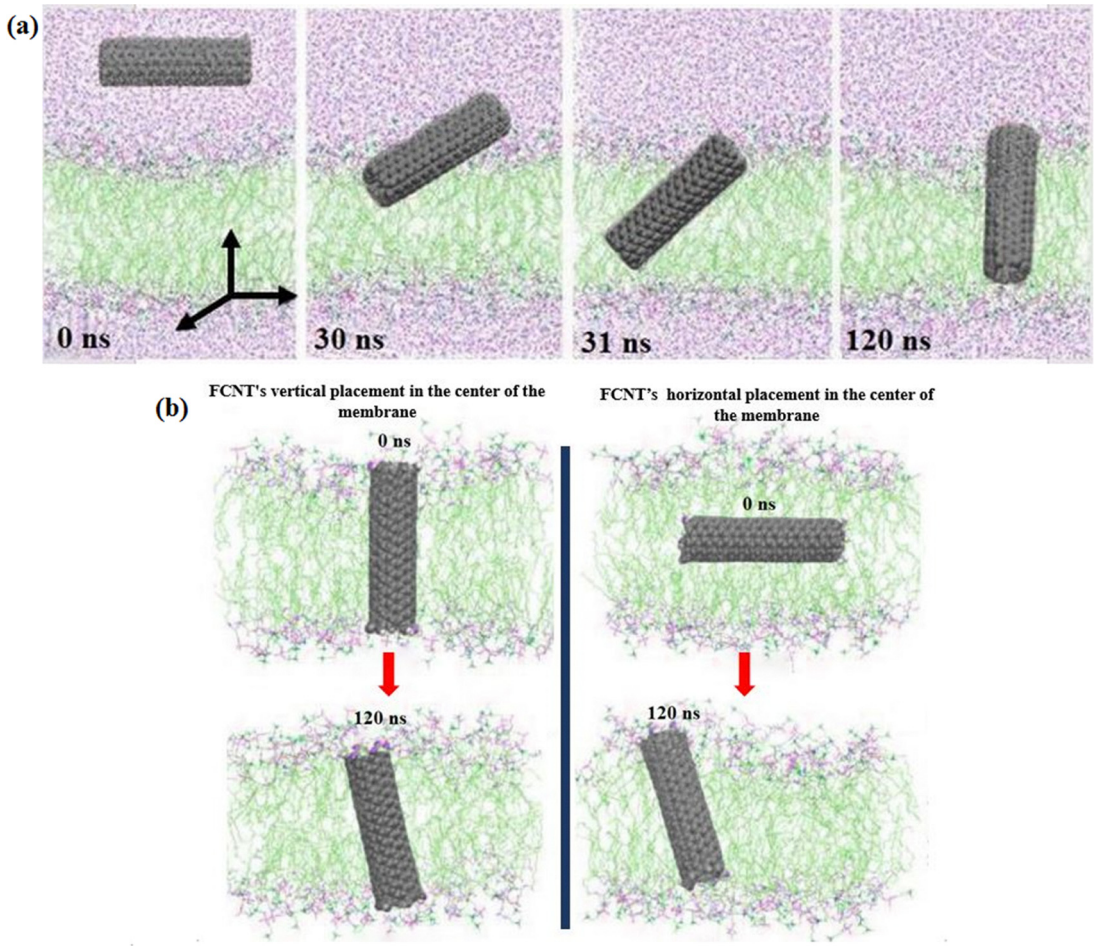


Fig. 6 (a) The path of CNT–COOH entering the membrane and (b) the path of CNT–COOH located in the membrane vertically and horizontally (pictures at $t$ = 0 ns and $t$ = 120 ns).

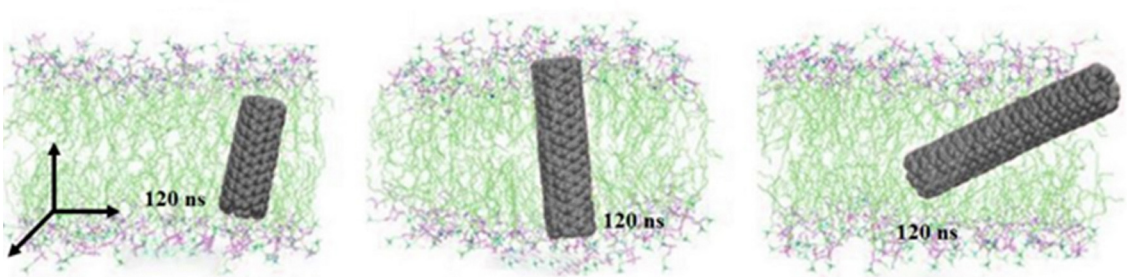


Fig. 7 Final times (120 ns) of pristine CNTs with different lengths (from left to right 2.6 nm, 3.8 nm, and 5 nm, respectively) entering the membrane.

molecules to traverse the membrane.[25,67] Conversely, longer CNTs experience greater steric hindrance and are less able to rotate. This reduced mobility can lead to misalignment or partial insertion, where only a segment of the CNT is embedded within the membrane, potentially disrupting membrane integrity and reducing the efficiency of molecular transport. Furthermore, the aspect ratio of CNTs (length-to-diameter ratio) plays a significant role in their interaction with lipid bilayers. High aspect ratio CNTs, which are long and thin, tend to have more pronounced rotational dynamics and face greater difficulty achieving a stable orientation within the membrane. In contrast, CNTs with lower aspect ratios, which are shorter and thicker, can more easily adopt favorable orientations and maintain stability within the bilayer.[18,68]

It is believed that pristine CNTs can be rapidly placed into the lipid bilayer due to strong dispersion interactions with the lipid tails. To explore this phenomenon, we calculated the van der Waals interaction energy between pristine CNTs and the bilayer (Fig. 8a). The resulting energy curve indicated that these

 

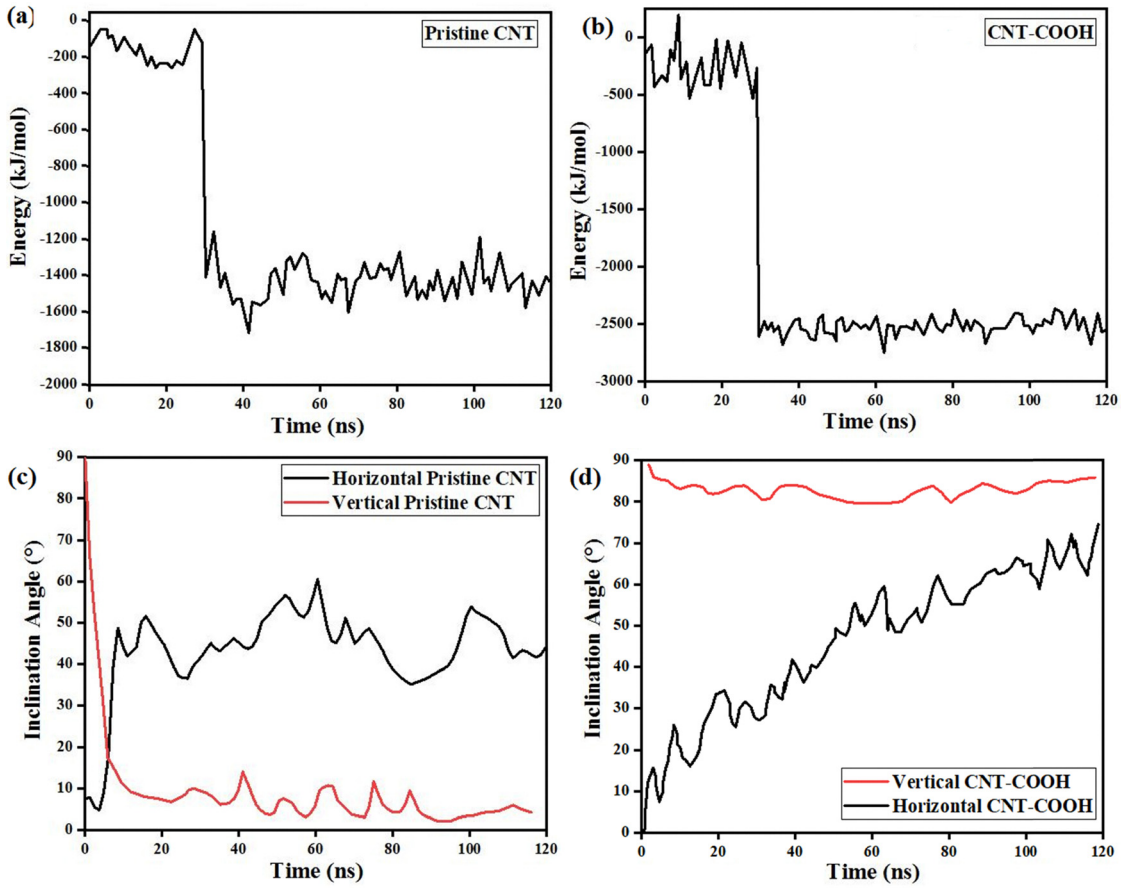


Fig. 8 (a) The time progression of the interaction energy between pristine CNTs and the membrane, (b) the time progression of the interaction energy between CNT–COOH and the membrane, (c) the alignment of pristine CNTs in horizontal and vertical positions in the cell membrane, and (d) the alignment of CNT–COOH in horizontal and vertical positions in the cell membrane.

interactions drove the translocation of pristine CNTs from the aqueous phase into the membrane. The energy difference between the pristine CNTs situated inside and outside the bilayer was found to be approximately 1100 kJ $mol^{-1}$. This great energy difference facilitated the swift adsorption of pristine CNTs into the lipid bilayer. When CNT–COOH interacted with the cell membrane, the interaction energy was typically enhanced compared to the pristine CNTs due to the presence of polar or charged functional groups (Fig. 8b). Functionalization often introduces polar or charged groups to the CNTs, which can enhance their interaction with the lipid bilayer. This might lead to more negative interaction energies compared to the pristine CNTs (Fig. 8b). The energy difference between CNT–COOH situated inside and outside the bilayer was found to be approximately 2500 kJ $mol^{-1}$. The nature of the functional groups might introduce specific interactions with the lipid bilayer components. This could result in a stronger orientation dependence of the interaction energy, as certain angles might favor the interaction of functional groups with the bilayer. In summary, while pristine CNTs exhibit significant interaction energies with the lipid bilayers, CNT–COOH further enhance these interactions, potentially leading to even faster insertion and more specific orientation-dependent behavior within the membrane. This underscores the importance of functionalization in tailoring CNT properties for mass transfer applications through the cell membrane. Fig. 8c and d present an insightful examination of the inclination angles of both pristine CNTs and CNT–COOH within a membrane, respectively, focusing on their behavior across horizontal and vertical orientations over time. In the case of pristine CNTs (Fig. 8c), for the horizontal orientation, the inclination angle experiences a sharp initial increase followed by considerable fluctuations ranging from 30 to 60 degrees over time. This pattern suggests a degree of instability and variability in this orientation. Conversely, in the vertical orientation, the inclination angle of pristine CNTs stabilizes after an initial sharp drop, fluctuating within a narrower range of 0–20 degrees, indicating improved stability in this configuration. In contrast, Fig. 8d depicts the inclination angles of CNT–COOH. The red curve, representing vertical CNT–COOH, maintains a high and stable inclination angle close to 90 degrees throughout the entire time span, demonstrating a strong and consistent vertical alignment. The black curve for horizontal CNT–COOH begins at a lower inclination angle but shows a steady increase over time, indicating a gradual shift towards vertical alignment. These findings suggest that functionalized CNTs exhibit superior alignment properties

compared to the pristine CNTs, particularly in maintaining a vertical orientation within the membrane. The obtained results in this work show a good agreement with the previous reports.[18,24,69] Kraszewski *et al.*[70] employed molecular dynamics simulations and a statistical model to evaluate the capability of the functionalized CNTs for internalization within a model lipid bilayer as a function of their length. They found that hydrophobicity was a key factor in the process of membrane entry. Their results indicated that shorter nanotubes have a stronger tendency to passively penetrate the bilayers and reach the cytoplasm. Furthermore, studies conducted by Lacerda *et al.*[24] demonstrated that the electrostatic interactions between the hydrophilic functional groups of functionalized CNTs and the polar head groups of lipid membranes were the primary drivers in the absorption and penetration of CNTs into the cell membrane. Kiani *et al.*[71] investigated the interactions of the pristine and functionalized CNTs with a cell membrane model. The MDS results showed that, in all systems, CNTs moved spontaneously from the aqueous phase to the center of the membrane *via* a "nanoneedle" mechanism. The types of the functional groups on the CNTs significantly affected the penetration into the lipid membrane. The interactions of the functionalized CNTs with the membrane headgroups increased due to the presence of the functional groups on the CNT surfaces. The van der Waals interaction energy for the pristine CNTs, CNTs with amine groups, and CNTs with carboxylic acid groups reached −1059, −1180, and −1255 kJ mol$^{-1}$, respectively, indicating that CNTs with carboxylic acid groups have stronger interactions with the lipid bilayer compared to the other types of CNTs.

### 3.5. The effectiveness of CNTs as artificial membrane channels

The influence of CNTs as artificial membrane channels on *n*-decane uptake by the bacterial cells was investigated. Fig. 9 illustrates the percentage of *n*-decane uptake for the two species, *Bacillus subtilis* and *Pseudomonas aeruginosa*, across three different systems: microbial control without CNTs, microbial broth with CNT–COOH, and the broth with pristine CNTs. As can be seen, in the microbial control system, *Bacillus subtilis* showed approximately 12% *n*-decane uptake, whereas *Pseudomonas aeruginosa* exhibited a higher transfer percentage at around 18%. The system containing CNT–COOH significantly enhanced *n*-decane uptake for both species, while the hydrocarbon content of *Bacillus subtilis* cells was assayed around 32% and that of *Pseudomonas aeruginosa* cells was about 41%. In the pristine CNT system, the uptake percentages were around 25% for *Bacillus subtilis* and 30% for *Pseudomonas aeruginosa*. Although CNT treatments could affect viability to some extent, the hydrocarbon uptake assay was performed under short exposure times with identical initial inoculums. To clarify the point, it should be mentioned that the sole carbon source for bacterial growth in the uptake experiments was hydrocarbons. The bacterial cell growth rate on this poorly aqueous soluble source is by far lower than that on the conventional culturing media such as the nutrient broth, which was used in the viability experiments. Our previous studies showed that the growth of the employed bacteria (*i.e. Pseudomonas aeruginosa* and *Bacillus subtilis*) on hydrocarbons in the first 12 hours was very low.[26,75] As a result, the 12-hour exposure can be considered as a short time because the bacterial cell density during this time would not increase largely. Accordingly, the uptake percentages were mainly measures of differences in membrane permeability, not biomass. Moreover, the control samples that contain bacteria without any types of CNTs showed a much lower hydrocarbon uptake level than the samples with CNTs (Fig. 9) despite the fact that in the absence of CNTs the population of viable bacteria would be higher. This approves the effectiveness of CNTs in increasing the cell wall permeability to the hydrocarbons in the presence of CNTs, which can be considered more efficient than the cell population. On the other hand, the viability experiments showed that (Fig. 2 and 3) the growth of *Pseudomonas aeruginosa* and *Bacillus subtilis* cells treated with CNT–COOH was around 13% and 40% higher than that of the cells exposed to pristine CNTs. Meanwhile, the hydrocarbon uptake in these two systems for *Pseudomonas aeruginosa* and *Bacillus subtilis* increased 27% and 21%, respectively. Clearly, the increase in the cell viability for *Bacillus subtills* cells in the CNT–COOH system (40%) has not led to a proportional rise in its hydrocarbon uptake and *Pseudomonas aeruginosa* with a lower viability improvement (13%) showed a higher uptake rise (27%). This means that the interactions between the cell wall and CNTs can be considered as a more important factor than the cell density. The inclusion of error bars indicated that there were some variabilities in the measurements, but the overall trend showed that *Pseudomonas aeruginosa* consistently exhibited a higher percentage of *n*-decane uptake compared to *Bacillus subtilis* across all systems. The results of visualization by TEM (Fig. 4 and 5) revealed that *Pseudomonas* bacterial cells had a more intensive interaction with CNTs as the number of CNTs absorbed to their cells were higher than that in the case of *Bacillus subtilis*. This means that the number of artificial channels in the *Pseudomonas* species membranes was higher,

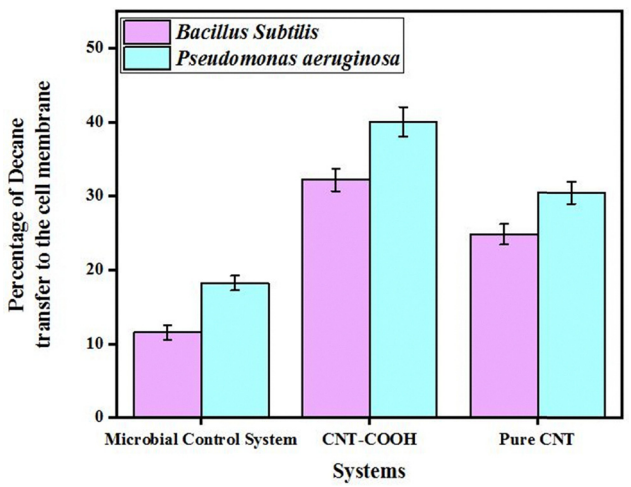


Fig. 9 The capability of pristine CNTs and CNT–COOH as artificial channels in transferring decane to the cell membrane for both *Bacillus subtilis* and *Pseudomonas aeruginosa* strains.

which led to greater amounts of hydrocarbon uptake. Moreover, the outer membrane of *Pseudomonas aeruginosa* is rich in lipopolysaccharides and interacts more effectively with hydrocarbons compared to the peptidoglycan-dominant cell walls of *Bacillus subtilis*.[72] In fact, this strain can import hydrocarbons *via* a pinocytosis mechanism, which is more efficient for the bulk internalization of hydrophobic substrates such as *n*-decane. Additionally, *Pseudomonas aeruginosa* exhibits metabolic versatility, equipped with specific transport proteins and mechanisms for hydrocarbon uptake and assimilation,[73] resulting in enhanced *n*-decane transfer rates. Its capability for biofilm formation further augments this process, as biofilms create microenvironments that concentrate hydrocarbons, making them more accessible for cellular uptake. Furthermore, *Pseudomonas aeruginosa* typically has a more hydrophobic cell surface, promoting the adherence and partitioning of hydrophobic compounds into the cell membrane. These structural and genetic adaptations collectively contribute to the superior efficiency of *Pseudomonas aeruginosa* in incorporating decane into the cell membrane compared to *Bacillus subtilis* in the different systems examined.

The CNT–COOH system proved to be the most effective in facilitating *n*-decane transfer through the cell membranes of both bacterial species, followed by the pristine CNT system, which also enhanced the transfer compared to the control system. The superior efficacy of the CNT–COOH system can be explained by several factors related to the functionalization of CNTs. First and foremost, it was revealed in the modelling section that the alignment of carboxylated CNTs in the lipid bilayer was perpendicular to the membrane plane, which was optimal for the construction of nanochannels. Therefore, the CNT–COOH channels would result in the most significant improvement in hydrocarbon uptake into the cells. Secondly, the introduction of carboxyl (COOH) groups to CNTs enhances their hydrophilicity and dispersibility in aqueous environments, increasing the interaction surface between the CNTs and bacterial cell membranes.[30,74] Pristine CNTs tend to aggregate in aqueous environments, reducing their effective surface area and interaction potential with bacterial membranes. Thirdly, without the COOH functional groups, pristine CNTs also have fewer sites for hydrogen bonding and electrostatic interactions with the cell membrane, resulting in a less efficient transfer process. Thus, the functionalization of CNTs with COOH groups significantly enhances their ability to facilitate decane transfer to bacterial cell membranes, making the CNT–COOH system the most effective among the systems examined. Results of the non-microbial control and the control without microorganisms and CNTs showed a small decrease in the hydrocarbon content of the flasks (less than 2%), which means that the absorption of hydrocarbons to CNTs or their evaporation was not significant in comparison to the other obtained results ($p < 0.05$). While statistical analyses of means were not performed pairwise, the differences between the control, CNT–COOH, and pristine CNT systems are greater than the experimental variability shown by the error bars. The trends were highly reproducible across independent replicates and are in line with the mechanistic behavior described.

The low kinetics of microorganisms in the biodegradation of hydrocarbons leads to a slow rate of bioremediation processes for the treatment of petroleum contamination. Despite the efforts to accelerate the process by a variety of methods (*e.g.*, higher cell populations, application of biosurfactants and promoting agents, cometabolic pathways, *etc.*),[75] the slow rate of the process still remains one of the most important disadvantages of bioremediation. Increasing the uptake capacity of the viable hydrocarbon assimilating cells by using modified CNTs as suggested in this work can convert the cells into fast and effective absorbents, which improve the rate of hydrocarbon removal in bioremediation processes.

Bioremediation efficiency can be significantly improved by the use of engineered nanostructures, which enhance the bioavailability, mass transfer, and uptake of hydrophobic contaminants.[76,77] Functionalized CNTs, such as CNT–COOH, play a key role in this process through several complementary mechanisms. First, due to their nanoscale tubular structure, they can act as artificial transmembrane channels, increasing the permeability of bacterial membranes to hydrophobic hydrocarbons and accelerating intracellular transport. Second, the improved dispersibility and reduced aggregation of functionalized CNTs increase their interaction with microbial cells, enabling them to function as nanoscale ''carriers'' that deliver hydrocarbons to the cell surface. Third, CNTs can locally concentrate hydrocarbons at the cell–nanotube interface, reducing mass-transfer limitations that typically restrict the biodegradation of poorly soluble compounds.[77] Furthermore, the lower cytotoxicity of CNT–COOH allows hydrocarbon-assimilating bacteria to maintain viability and metabolic activity during exposure, resulting in more efficient assimilation pathways. These combined physicochemical and biological mechanisms demonstrate how modified CNTs can enhance microbial bioremediation by accelerating hydrocarbon uptake, improving bioavailability, and ultimately increasing the biodegradation rate.[77,78]

While this research shows positive findings about CNT–COOH contributing to the enhancement of hydrocarbon uptake and supporting bioremediation, there are some limitations. First and foremost, the study was conducted under laboratory conditions and does not consider the full range of intricacies that field settings may provide regarding temperature, pH, and other pollutants that may affect the efficacy of CNTs. Additionally, this study examined only two bacterial species (*Bacillus subtilis* and *Pseudomonas aeruginosa*), and continued research is needed to further examine the performance of CNTs with other classes of microbes, as the interaction dynamics may differ between different microbial groups. Lastly, while the efficacy of CNT–COOH enhances hydrocarbon uptake, there is a need to evaluate the long-term toxicity and environmental implications of CNTs, especially through field applications. Future studies should attempt to address these limitations by examining a wider range of bacterial types, optimizing the properties of the CNTs, and/or assessing the long-term efficacy and safety of CNTs' bioremediation strategy in a broader range of environmental settings.

## 4. Conclusion

This study explored the potential of CNTs, particularly CNT–COOH, as artificial membrane channels to enhance the uptake of hydrophobic substances, such as hydrocarbons, by bacterial cells. Through a series of toxicity assays, bacterial growth measurements, hydrocarbon uptake experiments, and molecular dynamics simulations (MDS), we demonstrated that CNTs, especially when functionalized with carboxyl groups, offer significant advantages for improving bioremediation processes. Our results showed that CNT–COOH were more biocompatible than pristine CNTs, as they reduced cytotoxicity and facilitated the enhanced uptake of *n*-decane by both *Bacillus subtilis* and *Pseudomonas aeruginosa*. Specifically, CNT–COOH increased the intracellular concentration of *n*-decane to 32% in *Bacillus subtilis* and 41% in *Pseudomonas aeruginosa*. This enhancement in hydrocarbon uptake was a direct result of the CNTs' ability to form stable, nanoscale channels within bacterial membranes, as confirmed by MDS. These findings underscore the potential of functionalized CNTs as effective tools for accelerating hydrocarbon biodegradation, addressing the slow kinetics typically observed in bioremediation processes. Furthermore, we observed that *Pseudomonas aeruginosa*, with its Gram-negative cell wall, exhibited greater resistance to CNTs, which may suggest its higher adaptability to these nanostructures compared to *Bacillus subtilis*. Overall, the study highlights the potential of CNT–COOH in improving the bioavailability and transport of hydrophobic compounds, making them an attractive option for both bioremediation and drug delivery applications. However, future research should focus on further optimizing CNT properties, exploring their long-term stability, and minimizing potential toxicity in practical applications to maximize their efficacy and safety for environmental and biomedical applications.

## Author contributions

Sara Yazdani: investigation, software, data curation, writing – original draft, visualization, writing – review & editing. Davoud Biria: conceptualization, supervision, methodology, project administration, writing – review & editing. Gholamreza Pazuki: data curation, writing – original draft, writing – review & editing.

## Conflicts of interest

There are no conflicts to declare.

## Data availability

All data generated or analyzed during this study are included in this published article and its supplementary information (SI). Supplementary information is available. See DOI: https://doi.org/10.1039/d5ma01079a.

## Acknowledgements

The authors would like to thank the Iran National Science Foundation (INSF) and the University of Isfahan for funding this work through grant no. 4014348.

## References

1 E. D. Korn, *Annu. Rev. Biochem.*, 1969, **38**, 263–288.
2 S. Yazdani, S. M. Ghoreishi and N. Habibi, *Protein Pept. Lett.*, 2022, **29**, 80–88.
3 K. Niikura, K. Nambara, T. Okajima, Y. Matsuo and K. Ijiro, *Langmuir*, 2010, **26**, 9170–9175.
4 R. H. Amran, M. T. Jamal, A. Pugazhendi, M. Al-Harbi, M. Ghandourah, A. Al-Otaibi and M. F. Haque, *Nat. Environ. Pollut. Technol.*, 2022, **21**(3), 1149–1157.
5 A. Kalia, S. Sharma, N. Semor, P. K. Babele, S. Sagar, R. K. Bhatia and A. Walia, *3 Biotech*, 2022, **12**, 135.
6 S. Yazdani, M. Mozaffarian, G. Pazuki, N. Hadidi, I. Villate-Beitia, J. Zárate, G. Puras and J. L. Pedraz, *Pharmaceutics*, 2024, **16**, 288.
7 S. Yazdani, M. Mozaffarian, G. Pazuki and N. Hadidi, *Cell Signaling*, 2024, **2**, 148–154.
8 L. Lacerda, J. Russier, G. Pastorin, M. A. Herrero, E. Venturelli, H. Dumortier, K. T. Al-Jamal, M. Prato, K. Kostarelos and A. Bianco, *Biomaterials*, 2012, **33**, 3334–3343.
9 A. Verma, O. Uzun, Y. Hu, Y. Hu, H.-S. Han, N. Watson, S. Chen, D. J. Irvine and F. Stellacci, *Nat. Mater.*, 2008, **7**, 588–595.
10 T. Shimizu, W. Ding and N. Kameta, *Chem. Rev.*, 2020, **120**, 2347–2407.
11 J. H. Chung, N. Hasyimah and N. Hussein, *Trop. Aquat. Soil Pollut.*, 2022, **2**, 13–26.
12 S. Yazdani, D. Biria and G. Pazuki, *RSC Adv.*, 2025, **15**, 24624–24638.
13 H. Zare, S. Ahmadi, A. Ghasemi, M. Ghanbari, N. Rabiee, M. Bagherzadeh, M. Karimi, T. J. Webster, M. R. Hamblin and E. Mostafavi, *Int. J. Nanomed.*, 2021, 1681–1706.
14 H. Ijaz, A. Mahmood, M. M. Abdel-Daim, R. M. Sarfraz, M. Zaman, N. Zafar, S. Alshehery, M. M. Salem-Bekhit, M. A. Ali and L. B. Eltayeb, *Inorg. Chem. Commun.*, 2023, 111020.
15 B. P. Makhado, A. O. Oladipo, N. N. Gumbi, L. A. De Kock, C. Andraos, M. Gulumian and E. N. Nxumalo, *Toxicol. In Vitro*, 2024, 105898.
16 A. A. Mathew, M. Varghese and M. Balachandran, in *Carbon nanostructures in biomedical applications*, Springer, 2023, pp. 363–398.
17 M. Sianipar, S. H. Kim, F. Iskandar and I. G. Wenten, *RSC Adv.*, 2017, **7**, 51175–51198.
18 J. Geng, K. Kim, J. Zhang, A. Escalada, R. Tunuguntla, L. R. Comolli, F. I. Allen, A. V. Shnyrova, K. R. Cho and D. Munoz, *Nature*, 2014, **514**, 612–615.
19 C. Gao, M. Guo, Y. Liu, D. Zhang, F. Gao, L. Sun, J. Li, X. Chen, M. Terrones and Y. Wang, *Carbon*, 2023, **212**, 118133.

20 C. Sebaaly, H. Greige-Gerges and C. Charcosset, in *Current trends and future developments on (bio-) membranes*, Elsevier, 2019, pp. 311–340.
21 X. Wang, H. Du, Z. Wang, W. Mu and X. Han, *Adv. Mater.*, 2021, **33**, 2002635.
22 S. Kang, M. Pinault, L. D. Pfefferle and M. Elimelech, *Langmuir*, 2007, **23**, 8670–8673.
23 C. D. Vecitis, K. R. Zodrow, S. Kang and M. Elimelech, *ACS Nano*, 2010, **4**, 5471–5479.
24 L. Lacerda, H. Ali-Boucetta, S. Kraszewski, M. Tarek, M. Prato, C. Ramseyer, K. Kostarelos and A. Bianco, *Nanoscale*, 2013, **5**, 10242–10250.
25 A. A. Skandani, R. Zeineldin and M. Al-Haik, *Langmuir*, 2012, **28**, 7872–7879.
26 R. Barin, M. Talebi, D. Biria and M. Beheshti, *Int. J. Environ. Sci. Technol.*, 2014, **11**, 1701–1710.
27 S. Yazdani, M. Mozaffarian, G. Pazuki, N. Hadidi, I. Gallego, G. Puras and J. L. Pedraz, *Sci. Rep.*, 2022, **12**, 21114.
28 S. Yazdani, M. Mozaffarian, G. Pazuki and N. Hadidi, *J. Mol. Liq.*, 2022, **360**, 119519.
29 S. Ali, S. A. U. Rehman, H.-Y. Luan, M. U. Farid and H. Huang, *Sci. Total Environ.*, 2019, **646**, 1126–1139.
30 R. Dubey, D. Dutta, A. Sarkar and P. Chattopadhyay, *Nanoscale Adv.*, 2021, **3**, 5722–5744.
31 S. Bhuyan, M. Yadav, S. J. Giri, S. Begum, S. Das, A. Phukan, P. Priyadarshani, S. Sarkar, A. Jayswal and K. Kabyashree, *J. Microbiol. Methods*, 2023, **207**, 106707.
32 H. Chen, B. Wang, D. Gao, M. Guan, L. Zheng, H. Ouyang, Z. Chai, Y. Zhao and W. Feng, *Small*, 2013, **9**, 2735–2746.
33 A. T. Rogers, K. R. Bullard, A. C. Dod and Y. Wang, *Bio-Protoc.*, 2022, **12**, e4410–e4410.
34 V. R. Krishnamurthi, I. I. Niyonshuti, J. Chen and Y. Wang, *PLoS One*, 2021, **16**, e0245205.
35 T. Chatterjee, B. K. Chatterjee, D. Majumdar and P. Chakrabarti, *Biochim. Biophys. Acta (BBA)-Gen. Subj.*, 2015, **1850**, 299–306.
36 M. Poormontaseri, R. Ostovan, E. Berizi and S. Hosseinzadeh, *Int. J. Nutr. Sci.*, 2017, **2**, 39–42.
37 O. Berger, O. Edholm and F. Jähnig, *Biophys. J.*, 1997, **72**, 2002–2013.
38 G. Hummer, J. C. Rasaiah and J. P. Noworyta, *Nature*, 2001, **414**, 188–190.
39 A. W. Schüttelkopf and D. M. Van Aalten, *Acta Crystallogr. Sect. D: Biol. Crystallogr.*, 2004, **60**, 1355–1363.
40 W. L. Jorgensen, J. Chandrasekhar, J. D. Madura, R. W. Impey and M. L. Klein, *J. Chem. Phys.*, 1983, **79**, 926–935.
41 H. J. Berendsen, D. van der Spoel and R. van Drunen, *Comput. Phys. Commun.*, 1995, **91**, 43–56.
42 B. Hess, C. Kutzner, D. Van Der Spoel and E. Lindahl, *J. Chem. Theory Comput.*, 2008, **4**, 435–447.
43 T. Darden, D. York and L. Pedersen, *J. Chem. Phys.*, 1993, **98**, 10089–10092.
44 U. Essmann, L. Perera, M. L. Berkowitz, T. Darden, H. Lee and L. G. Pedersen, *J. Chem. Phys.*, 1995, **103**, 8577–8593.
45 B. Hess, H. Bekker, H. J. Berendsen and J. G. Fraaije, *J. Comput. Chem.*, 1997, **18**, 1463–1472.
46 S. Miyamoto and P. A. Kollman, *J. Comput. Chem.*, 1992, **13**, 952–962.
47 S. Park and K. Schulten, *J. Chem. Phys.*, 2004, **120**, 5946–5961.
48 J. S. Hub, B. L. De Groot and D. Van Der Spoel, *J. Chem. Theory Comput.*, 2010, **6**, 3713–3720.
49 A. E. D. R. Castillo, A. De León-Rodriguez, M. Terrones and A. P. B. de la Rosa, *Carbon*, 2021, **184**, 902–909.
50 S. Brown, A. Jorio, M. Dresselhaus and G. Dresselhaus, *Phys. Rev. B*, 2001, **64**, 073403.
51 S. V. Sawant, A. W. Patwardhan, J. B. Joshi and K. Dasgupta, *Chem. Eng. J.*, 2022, **427**, 131616.
52 A. C. Ferrari and D. M. Basko, *Nat. Nanotechnol.*, 2013, **8**, 235–246.
53 M. Amin, B. M. Abdullah, S. J. Rowley-Neale, S. Wylie, A. J. Slate, C. E. Banks and K. A. Whitehead, *Sensors*, 2022, **22**, 675.
54 B. De Menezes, F. Ferreira, B. Silva, E. Simonetti, T. Bastos, L. Cividanes and G. Thim, *J. Mater. Sci.*, 2018, **53**, 14311–14327.
55 C. K. Thakur, R. Neupane, C. Karthikeyan, C. R. Ashby Jr, R. J. Babu, S. H. Boddu, A. K. Tiwari and N. S. H. N. Moorthy, *Molecules*, 2022, **27**, 7461.
56 F. J. Peón-Díaz, R. S. del Río, S. Hevia, F. Olivares, J. C. Expósito-Gálvez, R. Escalante, K. Valadez-Villalobos, A. J. Riquelme, G. Oskam and R. Henríquez, *J. Mater. Sci.*, 2023, **58**, 5372–5388.
57 A. Augustyniak, K. Dubrowska, J. Jabłońska, K. Cendrowski, R. J. Wróbel, M. Piz, E. Filipek and R. Rakoczy, *Appl. Nanosci.*, 2022, **12**, 1917–1927.
58 Y. Maksimova, Y. Bykova and A. Maksimov, *Microorganisms*, 2022, **10**, 1627.
59 J. Dong, B. Wang, B. Xiang, J. Yang, Z. Gong, Z. Wang, Y. Huang and L. Chen, *J. Clin. Lab. Anal.*, 2020, **34**, e23417.
60 M. A. Saleemi, M. H. Fouladi, P. V. C. Yong and E. H. Wong, *Materials*, 2020, **13**, 1676.
61 S. E. Abo-Neima, H. A. Motaweh and E. M. Elsehly, *IET Nanobiotechnol.*, 2020, **14**, 457–464.
62 M. Anwar, F. Muhammad, B. Akhtar, M. I. Anwar, A. Raza and A. Aleem, *Int. J. Pept. Res. Ther.*, 2021, **27**, 1689–1697.
63 V. Pérez-Luna, C. Moreno-Aguilar, J. L. Arauz-Lara, S. Aranda-Espinoza and M. Quintana, *Sci. Rep.*, 2018, **8**, 17998.
64 Y. A. Attia, A. M. Al Nazawi, H. Elsayed and M. W. Sadik, *Saudi J. Biol. Sci.*, 2021, **28**, 484–491.
65 M. Sajid, M. Asif, N. Baig, M. Kabeer, I. Ihsanullah and A. W. Mohammad, *J. Water Process Eng.*, 2022, **47**, 102815.
66 A. R. Deline, B. P. Frank, C. L. Smith, L. R. Sigmon, A. N. Wallace, M. J. Gallagher, D. G. Goodwin Jr, D. P. Durkin and D. H. Fairbrother, *Chem. Rev.*, 2020, **120**, 11651–11697.
67 S. Baoukina, L. Monticelli and D. P. Tieleman, *J. Phys. Chem. B*, 2013, **117**, 12113–12123.
68 A. TermehYousefi, S. Bagheri, S. Shahnazar, M. H. Rahman and N. A. Kadri, *Mater. Sci. Eng.: C*, 2016, **59**, 636–642.
69 C. Corredor, W.-C. Hou, S. A. Klein, B. Y. Moghadam, M. Goryll, K. Doudrick, P. Westerhoff and J. D. Posner, *Carbon*, 2013, **60**, 67–75.

70 S. Kraszewski, F. Picaud, I. Elhechmi, T. Gharbi and C. Ramseyer, *Carbon*, 2012, **50**, 5301–5308.
71 M. F. Kiani, A. Zaboli, V. Shirshahi and H. Hashemzadeh, *Appl. Surf. Sci.*, 2023, **623**, 157039.
72 J. Ude, V. Tripathi, J. M. Buyck, S. Söderholm, O. Cunrath, J. Fanous, B. Claudi, A. Egli, C. Schleberger and S. Hiller, *Proc. Natl. Acad. Sci.*, 2021, **118**, e2107644118.
73 L. Molina, A. Segura, E. Duque and J.-L. Ramos, in *Advances in applied microbiology*, Elsevier, 2020, vol. 110, pp. 149–180.
74 Y. G. Maksimova, *Appl. Biochem. Microbiol.*, 2019, **55**, 1–12.
75 M. Karimi and D. Biria, *Chemosphere*, 2016, **152**, 166–172.
76 B. Kumari and D. Singh, *Ecol. Eng.*, 2016, **97**, 98–105.
77 E. Vázquez-Núñez, C. E. Molina-Guerrero, J. M. Peña-Castro, F. Fernández-Luqueño and M. G. de la Rosa-Álvarez, *Processes*, 2020, **8**, 826.
78 G. Rando, S. Sfameni, M. Galletta, D. Drommi, S. Cappello and M. R. Plutino, *Molecules*, 2022, **27**, 4856.